Published in final edited form as:
Exp Neurol. 2012 December ; 238(2): 284–296. doi:10.1016/j.expneurol.2012.08.015.

Effects of heat shock protein 72 (Hsp72) on evolution of astrocyte activation following stroke in the mouse

George E. Barreto, PhD[1,2], **Robin E. White, PhD**[1], **Lijun Xu, MD**[1], **Curtis J. Palm, PhD**[1,3], and **Rona G. Giffard, PhD, MD**[1]

[1]Department of Anesthesia, Stanford University School of Medicine, 300 Pasteur Drive, Stanford, CA 94305

[3]Stanford Genome Technology Center, Stanford University, 855 S. California Avenue, Palo Alto, CA 94304

Abstract

Astrocyte activation is a hallmark of the response to brain ischemia consisting of changes in gene expression and morphology. Heat shock protein 72 (Hsp72) protects from cerebral ischemia, and although several protective mechanisms have been investigated, effects on astrocyte activation have not been studied. To identify potential mechanisms of protection, microarray analysis was used to assess gene expression in the ischemic hemispheres of wild-type (WT) and Hsp72-overexpressing (Hsp72Tg) mice 24 hours after middle cerebral artery occlusion or sham surgery. After stroke both genotypes exhibited changes in genes related to apoptosis, inflammation, and stress, with more downregulated genes in Hsp72Tg and more inflammation-related genes increased in WT mice. Genes indicative of astrocyte activation were also upregulated in both genotypes. To measure the extent and time course of astrocyte activation after stroke, detailed histological and morphological analyses were performed in the cortical penumbra. We observed a marked and persistent increase in glial fibrillary acidic protein (GFAP) and a transient increase in vimentin. No change in overall astrocyte number was observed based on glutamine synthetase immunoreactivity. Hsp72Tg and WT mice were compared for density of astrocytes expressing activation markers and astrocytic morphology. In animals with comparable infarct size, overexpression of Hsp72 reduced the density of GFAP- and vimentin-expressing cells, and decreased astrocyte morphological complexity 72 h following stroke. However, by 30 days astrocyte activation was similar between genotypes. These data indicate that early modulation of astrocyte activation provides an additional novel mechanism associated with Hsp72 overexpression in the setting of ischemia.

INTRODUCTION

Astrocytes are dynamically involved in synaptic transmission (Perea and Araque, 2007, Perea, et al., 2009), metabolic and ionic homeostasis (Dienel and Hertz, 2005), inflammation, and maintenance of the blood brain barrier (Ballabh, et al., 2004). Within the

Correspondence to: Rona Giffard, Ph.D., M.D., Department of Anesthesia, Stanford University School of Medicine, 300 Pasteur Drive, S272A, Stanford, CA 94305, rona.giffard@stanford.edu, Telephone: 650-725-8482, Fax: 650-725-8052.
[2]Current Address: Departamento de Nutrición y Bioquímica, Facultad de Ciencias, Pontificia Universidad Javeriana, Bogotá D.C., Colombia

central nervous system astrocytes respond to insults including infection, trauma, neurodegenerative disease, and ischemia by activation, or reactive astrogliosis, which involves changes in gene expression and morphology, and may lead to glial scar formation and cell proliferation (Correa-Cerro and Mandell, 2007, Eddleston and Mucke, 1993, Maragakis and Rothstein, 2006, Pekny and Nilsson, 2005, Sofroniew, 2005, Sofroniew, 2009). Astrocyte activation includes the morphological changes of hypertrophy of cellular processes and hyperplasia of the cell body, and gene expression changes including induction of glial fibrillary acidic protein (GFAP) and re-expression of the radial glial markers vimentin (Vim), nestin, and somewhat delayed expression of brain lipid binding protein (BLBP) (White and Jakeman, 2008). The intermediate filament network is very prominent in the main processes and soma of activated astrocytes (Bushong, et al., 2002, Bushong, 2004).

Ischemia and subsequent reperfusion cause increased production of reactive oxygen species (ROS) and oxidative stress (Niizuma, et al., 2009), one of the triggers of astrocyte activation (Pekny and Nilsson, 2005). Hsp72, a member of the 70 kDa class of molecular chaperones or heat shock proteins (Hsps) regulates both apoptotic and necrotic cell death (Giffard, et al., 2004, Parcellier, et al., 2003, Yaglom, et al., 2003) and when overexpressed is associated with reduced oxidative stress (Xu, et al., 2009, Zheng, et al., 2008). Previous studies showed that overexpressing Hsp72 protects from cerebral ischemia (Giffard, et al., 2008, Hoehn, et al., 2001, Lee, et al., 2006, Plumier, et al., 1997, Rajdev, et al., 2000, van der Weerd, et al., 2005, Xu, et al., 2009, Yenari, et al., 1998, Zheng, et al., 2008), but the effects of Hsp72 overexpression on overall gene expression and astrocyte activation following focal ischemia are not well understood.

To further assess the neuroprotective effects of Hsp72 overexpression, gene expression profiling was performed in wild-type (WT) and Hsp72 overexpressing (Hsp72Tg) mice. This analysis showed that many genes, including genes associated with astrocyte activation, are differentially expressed after ischemia, even when harvesting all cell types in the injured hemisphere. Among the differentially regulated genes in response to ischemia were 8 astrocyte genes largely involved in inflammation. The effect of Hsp72 overexpression on astrocyte activation in response to focal ischemia was then quantitated by cell counting and morphological analysis of astrocytes in the ischemic penumbra at different time points after stroke. This showed that astrocytes express a time-dependent activation profile, and astrocytes in Hsp72Tg mice have a significantly less-activated phenotype, independent of lesion size. These data demonstrate that astrocyte activation changes in the lesion penumbra over time, indicative of different astrocyte functions or phenotypes over a time course extending from hours to 30 days. Reduced early astrocyte activation in Hsp72Tg mice may contribute to the observed neuroprotection.

MATERIALS AND METHODS

Hsp72Tg mice

Adult male mice expressing a chimeric transgene of the rat-inducible Hsp72 gene under control of the chicken-β-actin promoter and human cytomegalovirus enhancer (Hsp72Tg) were originally produced by Dillmann and colleagues (Marber, et al., 1995) and back bred into the C57BL/6 background. The strain is maintained as a heterozygous transgenic (Tg) line. Tg and wild type littermates were used for experiments after genotyping by polymerase chain reaction (PCR) analysis of tail DNA. C57BL/6 mice were purchased from Charles River Laboratories (Wilmington, MA, USA).

Focal Cerebral Ischemia

Transient ischemia was induced using the suture occlusion technique, as previously described (Han, et al., 2009), with slight modifications. Male mice 25±5g aged 2–4 months were anesthetized, and the left carotid artery bifurcation was exposed. A 6–0 monofilament nylon suture (Doccol Co., Redlands, CA, USA) was inserted from the common carotid artery (CCA) into the internal carotid artery to occlude the left middle cerebral artery (MCA) at its origin. After 60 min the suture was removed for reperfusion, the CCA ligated, and the wound closed. Sham-operated animals underwent identical procedures as far as isolation of the carotid bifurcation but without opening the artery or suture insertion. Rectal temperature was maintained at 37°C±0.5°C controlled by a Homeothermic blanket control unit (Harvard Apparatus, Holliston, MA, USA). Temperature and respiratory rate were monitored during the surgery, the duration of which was always 20 min. Infarct volumes are generally 35–45% of the hemisphere (Xiong, et al., 2011).

Preparation of microarray samples

C57BL/6 and Hsp72Tg mice were deeply anesthetized with isofluorane and sacrificed 24h after MCAO or sham surgery. Brains were rapidly removed, divided into hemispheres and RNA was extracted from the ischemic hemisphere or for sham animals the ipsilateral hemisphere using Qiagen RNeasy® Midi kit (Alameda, CA, USA). Total RNA samples were processed at the Stanford Protein and Nucleic Acid Biotechnology Facility by one-cycle target preparation, labeling, and hybridization to Affymetrix 430_2® (Affymetrix, Santa Clara, CA) whole genome mouse arrays, according to the manufacturer's protocol. Three animals were analyzed for each genotype at 24 h perfusion after MCAO, and two animals of each genotype for sham.

Microarray data analysis

Raw image files were processed using Affymetrix GCOS software. The Significance Analysis of Microarrays (SAM) method (Tusher, et al., 2001) was used to determine genes that were significantly differentially expressed between WT and Hsp72Tg and those differentially expressed between sham and MCAO conditions. For SAM analysis (Tusher, et al., 2001) initial chip processing and signal calling was done with R (http://rss.acs.unt.edu/Rdoc/library/siggenes/html/sam.html) and Bioconductor (Gentleman, et al., 2004) using the Affymetrix package (Gautier, et al., 2004). The RMA background correction method, quantile normalization and the median polish probe set summary method were employed. Differentially expressed genes were those with a fold-change of ≥ 2.0 and a p value of < 0.05. Data sets are posted at the Gene Expression Omnibus (GSE#28731). A current gene assignment for the Affymetrix probe sets was done using the Gene ID conversion tool on the DAVID bioinformatic resource (http://david.abcc.ncifcrf.gov/) (Dennis, et al., 2003, Huang da, et al., 2009). To determine over- and under-represented gene ontology (GO) categories, the lists of all genes showing ≥ 2 fold change and $p < 0.05$ for each genotype were uploaded and analyzed with the PANTHER Gene Expression Data Analysis tools on the PANTHER web site (http://www.pantherdb.org) (Thomas, et al., 2003, Thomas, et al., 2006). The expected number of genes is calculated from the percentage of genes from the mouse genome in each category and the number of differentially expressed genes used for the analysis. A p-value cutoff of 0.05 was chosen to identify over-represented GO categories.

Tissue Fixation and Immunohistochemistry

At 3, 6, 12, and 24h, 2, 3, 7, 14 and 30 days after stroke or sham-operation, mice were sacrificed for analysis. Animals were deeply anesthetized with isofluorane, and perfused through the left cardiac ventricle, first with 0.9% cold saline and then with 4% paraformaldehyde in phosphate-buffered saline (PBS) (pH 7.4). Brains were removed and

immersed for 2 days at 4°C in the same fixative and then rinsed with PBS. Coronal sections, 40 μm thick, were made with a Vibratome (VT 1000 S; Leica Microsystems, Wetzlar, Germany).

Immunofluorescence

Immunohistochemistry was carried out on free-floating sections under moderate shaking. Sections were incubated for 1h in blocking solution (0.1M PBS, 0.3% Triton X-100 and 5% equine serum). After three washes in 0.1M PBS, sections were incubated for 3 days at 4°C with primary antibody for glial fibrillary acidic protein (GFAP, diluted 1:5, #22522, Immunostar, Hudson, WI, USA), vimentin (diluted 1:100, sc-7557, Santa Cruz Biotechnology, CA), or brain lipid binding protein (BLBP, diluted 1:400, #32423, Abcam, Cambridge, MA). After incubation with primary antibody, sections were rinsed in buffer and incubated for 2h at room temperature with Alexa Fluor 488- (for GFAP) or 594- (for vimentin and BLBP) conjugated secondary antibodies (diluted 1:300, Invitrogen, Carlsbad, CA), washed three times in PBS, and mounted on glass slides using Vectashield mounting medium with 4′,6-diamidino-2-phenylindole (DAPI; Vector Laboratories, Burlingame, CA, USA).

Immunoperoxidase

All washes and incubations were done in washing buffer containing 0.1M PBS, 0.3% BSA and 0.3% Triton X-100. After 1h in blocking solution endogenous peroxidase activity was quenched for 10 min at room temperature in 3% hydrogen peroxide in 30% methanol. After several washes, sections were incubated for 3 days at 4°C with a polyclonal anti-rabbit antibody for S100β (diluted 1:200, Z0311, DAKO, Carpinteria, CA), or a monoclonal antibody for glutamine synthethase (GS, diluted 1:100, MAB302, Millipore, Bedford, MA). After incubating sections with primary antibody, sections were rinsed and incubated with biotinylated goat anti-rabbit immunoglobulin G (diluted 1:300, BA-1000 Vector Laboratories, Burlingame, CA, USA) or biotinylated horse anti-mouse immunoglobulin G (diluted 1:300, BA-2000, Vector Laboratories). After several washes in buffer, sections were incubated for 90 min at room temperature with avidin–biotin-peroxidase complex (diluted 1:250, ImmunoPure ABC peroxidase staining kit, Pierce, Rockford, IL, USA), then incubated with 2 μg/ml 3,3′-diaminobenzidine (Sigma-Aldrich) and 0.01% hydrogen peroxide in 0.1 M phosphate buffer. Sections were then dehydrated, mounted on gelatinized slides and observed with a Zeiss 200M Axiovert microscope (Zeiss, Germany).

Morphometric analysis

Brains that showed a similar infarcted area were used for morphometry to avoid the confound of differing extents of injury. The border between normal appearing cells and infarcted tissue is readily identified after 24 h (Dingman, et al., 2006) by the morphological appearance of nuclei. The core was identified as the region in which the majority of DAPI stained nuclei were shrunken, whereas the penumbra was defined as the region of generally morphologically normal cells, approximately 500 μm wide, surrounding the core, on brains through day 7. In brains 14 and 30 days after MCAO the penumbra was identified as the area outside of the relatively acellular infarct core which is delimited by the glial scar. The number of GFAP, Vimentin, S100β, and GS immunoreactive astrocytes was assessed in the layer II–III cortical penumbra of at least 3 animals (−1.70 to −2.18 mm relative to Bregma), covering a distance of 283 μm from the border of the ischemic core. The number of immunoreactive cells for the time course study was estimated using the fractionator disector method using manual counting of the number of immunopositive cells in an area of 0.08 mm^2 (283 μm × 283 μm) in the lesion penumbra using Image J software (USA National Institutes of Health http://rsb.info.nih.gov/ij/), 2–3 sections were counted and averaged per

mouse (Barreto, et al., 2011). For comparisons between WT and Hsp72Tg mice the number of immunoreactive cells was assessed within 150 μm of the core for better visualization at 40X magnification using a Zeiss LSM 510 META inverted laser scanning confocal microscope (Zeiss, Germany). Z-stacks of 5 planes with 2 μm spacing were recorded in 2 min intervals. The number of immunoreactive cells was counted, and a total of 24 counting frames were assessed per animal using Image J software. All counts were performed on coded sections so the investigator was blinded to the treatment group and genotype.

Morphological (fractal) analysis

Preselection of astrocytes: The $GFAP^+$ astrocytes examined for detailed morphological assessment were located within the cortical penumbra at a distance of 400 μm from the ischemic core. Cells were selected randomly using a scale generated automatically (available at http://www.random.org/integers). To analyse a sufficient number of cells in the sham condition, where very few GFAP+ astrocytes are identified, multiple additional sections were evaluated to obtain a number of cells comparable to the time points after MCAO.

Image Acquisition: Black and white images of $GFAP^+$ astrocytes were obtained using a digital camera on a Zeiss Axiovert inverted fluorescence microscope. The images were processed with Image J software. Using a 20X objective, cells were picked randomly in the same area selected for immunostaining, and the binary overlay of a cell was created by thresholding. All pixels above the threshold value were treated as belonging to the cell image. For each cell the appropriate threshold value was defined manually at the level at which the binary overlay completely covered the whole cell body and processes. Finally, the binary silhouette of the whole cell was reduced to its one-pixel outline for estimation of the fractal dimensions with the FracLac 2.5 ImageJ plug-in (Karperien, A., FracLac for ImageJ, version 2.5. http://rsb.info.nih.gov/ij/plugins/fraclac/FLHelp/Introduction.htm. 1999–2007).

Quantitative fractal analysis: Fractal analysis was carried out on binary images using the dilation method. With this method, each pixel in the cell outline was replaced with a disk of a diameter varying from 3–61 pixels. Then the area of the widened outline divided by the diameter of structuring element was plotted against this diameter on a log-log scale. The slope of the regression line (S) is related to the fractal dimension (D) by $D = 1 - S$. In addition, the following variables were measured in this study: the area of the cell silhouette (the cell area), and the arbor area – the area of the convex polygon obtained by connecting the tips of the longest astrocytic processes (also known as the convex hull area). We measured the solidity factor obtained by dividing the cell silhouette by the arbour area, and lacunarity, which measures heterogeneity to complement the fractal dimension in describing complexity.

Statistics: Data are expressed as mean ± SEM. The differences between groups were determined by *t*-test when only two groups were compared; differences between multiple groups were determined by analysis of variance followed by *post hoc* Dunnett's multiple comparison test when all conditions were compared to sham, and 2 way ANOVA was used for comparisons of two genotypes and times, using Graphpad Prism 5 (GraphPAD Software for Science, San Diego, CA, USA). Bonferroni *post hoc* tests were used to determine differences between genotypes after two-way ANOVA analysis. Differences were considered statistically significant for p-value <0.05.

RESULTS

Gene expression differences between sham and MCAO

RNA was prepared from the whole injured hemisphere, so gene expression changes in all cell types was assessed. For WT mice after MCAO the total number of genes meeting the 2-fold change and $p < 0.05$ criterion was 169, of which 161 were increased and 8 decreased relative to sham (Figure 1a, 1b). For Hsp72 overexpressors the total was 89 genes with 78 up and 11 down-regulated (Figure 1b; see full gene lists in Supplemental Table 1 and genes unique and shared in both genotypes in Supplemental Table 2). While the overall patterns were similar, there were more downregulated genes in the Hsp72Tg mice, and more upregulated genes than down regulated genes in both genotypes. To assess the types of molecular functions that were differentially regulated in response to MCAO, over-represented molecular function gene ontology (GO) categories were assessed in upregulated (Figure 1c) and downregulated (Figure 1d) genes. GO categories enriched in the up-regulated genes were primarily associated with chemokines, chaperones, macrophage activation, apoptosis, inflammation, and the p53 pathway. WT mice exhibited enhanced differential expression of genes associated with chemokines, macrophage activation, and inflammation, while Hsp72Tg mice showed enhanced differential expression of genes associated with the oxidative stress response. GO categories enriched in the down-regulated genes largely reflected receptors and cell signaling, with the Hsp72Tg mice having a significant number of genes related to neuronal action potential.

Gene expression differences between WT and Hsp72Tg mice

When we compared gene expression between genotypes within each condition, sham and MCAO separately, few differences were seen. In sham, only 1 gene was significantly different between genotypes, Cap1 (cyclase-associated protein 1), which was 20-fold increased in Hsp72Tg relative to WT. This gene has not been implicated in ischemia, though it is involved in schizophrenia (Wong, et al., 2005), behavioral sensitization after drug addiction (Iwazaki, et al., 2007), and neuronal ceroid lipofuscinoses (von Schantz, et al., 2008). After MCAO 2 genes, Sema3e (semaphorin 3e) and Lrrtm1 (leucine rich repeat transmembrane neuronal 1) were significantly different between genotypes, both decreased 2-fold in the Hsp72Tg mice relative to WT. Neither has yet been directly linked to ischemia.

Astrocyte related gene expression 1 day after MCAO

We noted that several genes associated with reactive astrocytes were upregulated from sham to MCAO in the gene expression data, so to better summarize this we created a list of astrocyte activation-related genes based on the literature that were also differentially regulated in response to stroke in our dataset. Twenty-five previously described genes came up on our list of differentially upregulated genes following MCAO. Fold changes of these genes are shown in Table 1. Many of the upregulated genes were associated with the inflammatory process triggered by injury, including *Cxcl2*, *Ccl2*, *Cxcl10*, *Cxcl1*, and *Il6*, which can be produced by astrocytes in response to stress. While in some of these cases pro-inflammatory gene expression increases were greater in the HspTg mice, they also showed greater increases of several anti-inflammatory astrocytic genes, such as *Socs3* and *Tgfbi*. Furthermore, several genes were differentially expressed in the WT, but not Hsp72Tg mice using our criteria, including *Spp1*, *Cd44*, *Cxcl2*, *Hmox1*, *Icam1*, *S100a11*, and *Thbs1*. In addition, while Hsp72Tg mice exhibited increased RNA expression of the intermediate filament proteins *Gfap* and *Vim*, unlike in WT these changes did not reach statistical significance.

Astrocyte activation with time after focal ischemia

Since gene expression changes associated with astrocyte activation were prominent in our expression dataset, we characterized astrocyte activation in the cortical penumbra in greater detail by immunostaining and morphological analysis as a function of time (Figure 2a,b). Sections immunostained for GFAP revealed an increased density of $GFAP^+$ astrocytes detectable by 3h after ischemia, and increasing strikingly and statistically significantly by 48h reaching a peak at 72h, with no further change at day 7, remaining markedly elevated through 1 month post-stroke (Figure 2c). In contrast, an increased density of Vim^+ astrocytes first appears 12–24h after stroke, reaching a peak by 72h and decreasing afterwards, returning to near basal levels by 1 month (Figure 2d).

Sections were also immunolabeled for glutamine synthetase (GS) and S100β, 2 other common astrocyte markers (Figure 3a,b). Quantification showed that GS cell density did not change significantly over time up to 1 month following stroke (Figure 3c). In contrast, the density of $S100\beta^+$ astrocytes increased modestly at 48h, peaked at 72h and decreased on day 7, returning to basal levels by 14d, not different from sham on day 14 and 30 (Figures 3d).

To further explore reactive astrocyte marker expression after stroke we immunolabeled for BLBP, a radial glial marker (Feng, et al., 1994). Expression of BLBP was limited to a few neuronal cells in sham and 24 h post MCAO brain (data not shown), but highly colocalized with GFAP 48 and 72h post injury (Figure 4a, 72h shown). Quantitation showed that the number of BLBP+ astrocytes increased significantly in the penumbra at 48 h, peaking at 72 h and remaining high through day 30 (Figure 4b,c). Overall the time course of changes in expression of the 5 astrocytic markers we assessed demonstrated 4 distinct patterns over time (Figure 5), indicating different stages or phenotypes of activated astrocytes. GFAP and BLBP both peaked at 3 days after surgery, and remained high through 30 days. While vimentin also peaked at 3 days, the density of cells expressing it declined rapidly and was back to baseline by 30 days. S100β showed modest changes at intermediate times only, being somewhat elevated only on days 2–7. Lastly, the number of GS positive cells did not change significantly, supporting the idea that the number of astrocytes does not change markedly in the penumbra following stroke, despite extensive changes in the number of cells expressing GFAP and Vim.

Morphological changes in astrocytes with time after focal ischemia

To quantitatively assess astrocyte morphology in response to ischemia we performed fractal analysis (Schaffner and Ghesquiere, 2001, Soltys, et al., 2001) of randomly selected individual astrocytes from the same area used for cell counting, and assessed cell and arbor area, fractal dimension, and lacunarity. $GFAP^+$ astrocytes assume a wide spectrum of forms, from small cells with short, thin and poorly ramified processes in sham-operated animals to large, extensively ramified cells after ischemia (Figure 6a). Cell complexity increases with time after focal ischemia, becoming statistically significant at 24h. After ischemia, the cell (Figure 6b) and arbor (Figure 6c) areas were larger than in sham, decreasing on days 14 and 30 back to baseline for arbor area. In the fractal dimension (Figure 6d), mean values were larger than those in sham. In contrast to cell area, this effect was mainly due to a reduction in the number of cells with small values of this parameter. High lacunarity values, indicating a decreased image density and increased gaps, or spaces between processes, are found in sham-operated animals, with similar or slightly lower lacunarity following MCAO that was only significantly lower at 24h-7d (Figure 6e).

Overexpression of Hsp72 decreases early astrocyte activation changes

Since GFAP was differentially increased in our microarray analysis between Hsp72Tg and WT mice following ischemia, we compared astrocyte activation between the genotypes.

Sections immunostained for GFAP, S100β, or vimentin showed a lower cellular density in the cortical penumbra in Hsp72Tg compared to WT mice (Figure 7a). Stereological assessment showed that overexpression of Hsp72 resulted in 33%, 39% and 35% fewer immunoreactive cells for GFAP (Figure 7b), vimentin (Figure 7c) and S100β (Figure 7d), respectively. In contrast, Hsp72 overexpression was associated with greater variability for some genes with a 35% increase in GS-immunoreactive cells at 72h (Figure 7e). On days 14 and 30, the number of GFAP, Vim, GS, or S100β immunoreactive astrocytes did not differ by genotype (data not shown). Density of BLBP positive cells did not differ between genotypes at any time point.

Hsp72 overexpression decreases morphological changes in astrocytes induced by MCAO

When assessed on day 3 following MCAO, not only was the number of $GFAP^+$ astrocytes lower (Figure 7b), but qualitative inspection showed differences in morphology compared to WT. Fractal cell complexity analysis revealed that Hsp72Tg astrocytes were thinner with shorter processes compared to WT astrocytes, with significantly smaller cell area (57%) and arbor area (59%), respectively (Figures 8a,b), and a 3% reduction in fractal dimension (Figure 8c). In contrast, lacunarity did not differ by genotype (Figure 8d).

DISCUSSION

Microarray analysis reveals immune and stress response-related genes upregulated after focal ischemia, with more downregulated genes in Hsp72Tg mice

After transient MCAO, we found that genes related to apoptosis, immune response, and stress response are upregulated after ischemia, in agreement with previous studies (Chen, et al., 2011, Tang, et al., 2002). Furthermore, we found a greater number of genes downregulated after ischemia in Hsp72Tg mice compared to WT mice, which exhibited few down-regulated genes. This is consistent with other protective treatments, such as ischemic preconditioning, that also exhibit more down-regulated genes after ischemia than control conditions (Stenzel-Poore, et al., 2004). Interestingly, comparison of genes downregulated in Hsp72Tg mice and those downregulated following ischemic preconditioning only yielded one shared gene, S100A6. Thus far, S100A6 has not been documented as a stroke-associated gene, but overexpression of S100A6 in astrocytes has been implicated both in Alzheimer's disease (Boom, et al., 2004) and amyotrophic lateral sclerosis (Hoyaux, et al., 2002), suggesting that decreased expression may be beneficial. The lack of additional shared genes between Hsp72Tg and ischemic preconditioned brains (Stenzel-Poore, et al., 2003) may be due to differences in the microarray chips used and/or mouse strain, in addition to biologically divergent pathways resulting in neuroprotection.

In addition, several astrocyte activation-related genes were differentially expressed in both genotypes following stroke. Almost all of these genes were also identified in our recent paper examining gene expression changes specifically in astrocytes following MCAO (Zamanian, et al., 2012), with the exceptions of S100a11 and Igfbp3 (Table 1). Our laboratory has observed an increase in these genes in an independent microarray experiment (unpublished data), but not in the study of isolated astrocytes, so although these genes can be expressed in astrocytes, the changes in expression from sham to MCAO observed here likely reflect changes in gene expression in other cell types. Similar to past microarray studies, we saw a significant increase in the well-characterized reactive astrocyte genes GFAP and vimentin (Sarabi, et al., 2008, Tang, et al., 2002) in WT, but these did not meet our statistical cut-off for Hsp72Tg mice, suggesting an attenuated activation in the Hsp72Tg genotype. In addition, multiple genes indicative of increased neuronal death were not differentially expressed in the Hps72Tg mice, such as CD44 (Wang, et al., 2002), Cxcl2 (De Paola, et al., 2007), and Thbs1 (Xing, et al., 2009). On the other hand, several astrocyte-

related genes were more up-regulated in the Hsp72Tg mice compared to controls, including IL-6. IL-6 is a pro-inflammatory cytokine that, although deleterious later after injury, exhibits a protective role acutely (Loddick, et al., 1998) and is considered a neuropoietic cytokine (Bauer, et al., 2007). While activated astrocytes are reported to produce IL-6 after ischemia (Lau and Yu, 2001), other cell types likely also upregulate IL-6 after stroke.

Hsp72 is increased in all cell types as the transgene is under the control of the β-actin promoter, thus protection of many cell types likely contributes to the overall protection seen in these mice. Increased Hsp72 is associated with protection of ventricular and endothelial function after ischemia-reperfusion injury (Currie, et al., 1988) and overexpression of Hsp72 in dorsal root ganglion cells increases survival following ischemic injury (Amin, et al., 1996), Thus far it is unclear whether Hsp72 overexpression in neurons alone would protect against cerebral ischemia. We have previously observed that overexpression of Hsp72 is protective against *in vitro* ischemic injury to astrocytes (Bergeron, et al., 1996) and that overexpression of Hsp72 when directed only to astrocytes can protect neurons from ischemia *in vitro* (Xu, et al., 1999) and in the intact brain (Xu, et al., 2010). In this paper we analyzed astrocyte activation in mice of both genotypes with similar sized infarcts, to eliminate a contribution due to differences in the extent of injury. Therefore, the differences in astrocyte activation observed likely directly reflect the effect of Hsp72 in the astrocytes.

Hsp72Tg mice exhibit a distinctive astrocyte response early following ischemia—The decreased density of GFAP, vimentin, and S100β-expressing astrocytes suggests that Hsp72Tg astrocytes have a less-reactive phenotype following MCAO. The importance of the observed increase in GS^+ cell density in Hsp72Tg mice at 72h is unclear. However, recent work found that inhibition of GS inhibits astrocytes' ability to take up glutamate, which may contribute to excitotoxicity (Zou, et al., 2010). Glutamate excitotoxicity has long been appreciated to contribute to ischemic cell death (Hirose and Chan, 1993, Lee, et al., 1999), so more astrocytes expressing GS may be another aspect of the neuroprotective effect of Hsp72-overexpression.

GFAP expression often correlates with severity of injury after ischemia, thus making it difficult to determine whether changes in astrocyte response are a cause or effect of neuronal death. In the current study, evaluation of astrocyte response to injury in WT versus Hsp72Tg mice was performed in brains identified as having comparable-sized infarcts in order to study the effect of Hsp72 independent of injury severity. Despite similar injuries, fewer astrocytes in Hsp72Tg mice expressed GFAP, vimentin, and S100β 72h after injury. Furthermore, fractal analysis revealed an astrocyte morphology closer to that of quiescent astrocytes in the Hsp72Tg mice. No differences in astrocyte protein expression or morphology were observed later, at 14 or 30 days after MCAO. Thus, astrocytes may play a key role in the neuroprotection exhibited in Hsp72Tg mice. In particular, modulating the early astrocyte response to injury may contribute to protection, as Hsp72Tg mice exhibit on average a decreased infarct size both acutely (Hoehn, et al., 2001) and chronically (Xu, et al., 2011). We previously demonstrated that astrocyte-specific overexpression of Hsp72 in global ischemia is neuroprotective (Xu, et al., 2010), and this study suggests that Hsp72-overexpressing astrocytes may also contribute to protection in focal ischemia.

The phenotype of astrocyte activation changes with time after ischemia—The observed alterations in reactive astrocyte-related genes suggest a different astrocyte phenotype in the Hsp72Tg mice compared to WT at early times, and a changing phenotype in the penumbra with time. This is the first quantitative assessment of the changes in density of astrocytes expressing these markers of reactivity with time after focal ischemia. Prior studies have identified changes in these proteins, but they did not quantitate changes in the number of cells expressing these proteins and did not assess them over time. Based on our

laboratory's previous work showing little astrocyte proliferation in the penumbra following MCAO (Barreto et al., 2011), it is likely that increases in GFAP-, vimentin-, and BLBP-positive astrocytes is primarily due to increased protein expression by resident astrocytes as opposed to increased cell division.

Consistent with prior studies in cerebral ischemia, and brain and spinal cord injury, we found GFAP upregulated within the first week, and the increase persisted chronically (Chiamulera, et al., 1993, Smith, et al., 1997, White, et al., 2010). We also observed a transient increase in vimentin expression early after injury, consistent with past studies in traumatic brain and spinal cord injury (Hausmann and Betz, 2001, White, et al., 2010) but not previously reported in ischemia. In addition, we report for the first time the time course for BLBP immunoreactivity after MCAO. BLBP-expressing astrocyte cell density shows a somewhat delayed increase relative to the other reactive astrocyte markers, and persists chronically. This differs from spinal cord injury where BLBP expression occurs even later, 7 days after injury, but also persists (White, et al., 2010). We did not observe a significant change in the number of GS cells in the injury penumbra of WT mice, consistent with previous observations showing only modest astrocyte proliferation following stroke (Barreto, et al., 2011, Fernaud-Espinosa, et al., 1993, Ridet, et al., 1997). Thus we observed that astrocytes have a distinct temporal pattern of marker expression after stroke, with astrocytes at 72h expressing GFAP and vimentin, but after 30 days expressing GFAP and BLBP, indicative of different phenotypes.

We observed that early reactive astrocytes transiently express vimentin, while the more chronic response is characterized by prolonged GFAP and BLBP expression. In addition to quantitating the density of astrocytes expressing each of these reactive proteins, we used fractal analysis to quantitate changes in astrocyte morphology over time. Although astrocyte hypertrophy has frequently been noted following ischemia and other traumatic CNS injuries, a careful examination of specific aspects of astrocyte morphology has not previously been reported for stroke. We show that cell area and process complexity change over time, which may also reflect functional differences in reactive astrocytes. The early astrocyte activation phenotype may indicate different functional activity compared to later activation, including glial scar formation. Previous work clearly suggests that reactive astrocytes may have both detrimental (Brambilla, et al., 2005, Fitch and Silver, 2008) and beneficial (Bush, et al., 1999, Hayakawa, et al., 2010) effects; for reviews see (Hamby and Sofroniew, 2010, Pekny and Nilsson, 2005), but more work is needed to better define different activated astrocyte phenotypes. This study provides a reliable baseline for beginning to define differences in astrocyte activation, as we demonstrate here following stroke in WT and Hsp72Tg mice.

Supplementary Material

Refer to Web version on PubMed Central for supplementary material.

Acknowledgments

The authors thank Dr. Bruce MacIver for critical review of the manuscript. This work was supported in part by NIH grant R01 GM49831 to RGG and NIH T32 GM089626 to REW.

References

1. Amin V, Cumming DVE, Latchman DS. Over-expression of heat shock protein 70 protects neuronal cells against both thermal and ischaemic stress but with different efficiencies. Neuroscience Letters. 1996; 206:45–48. [PubMed: 8848278]
2. Ballabh P, Braun A, Nedergaard M. The blood-brain barrier: an overview: Structure, regulation, and clinical implications. Neurobiology of Disease. 2004; 16:1–13. [PubMed: 15207256]

3. Barreto GE, Sun X, Xu L, Giffard RG. Astrocyte Proliferation Following Stroke in the Mouse Depends on Distance from the Infarct. PLoS ONE. 2011; 6:e27881. [PubMed: 22132159]
4. Bauer S, Kerr B, Patterson P. The neuropoietic cytokine family in development, plasticity, disease and injury. Nature reviews Neuroscience. 2007; 8:221–232.
5. Bergeron M, Mivechi NF, Giaccia AJ, Giffard RG. Mechanism of heat shock protein 72 induction in primary cultured astrocytes after oxygen-glucose deprivation. Neurological research. 1996; 18:64–72. [PubMed: 8714540]
6. Boom A, Pochet R, Authelet M, Pradier L, Borghgraef P, Van Leuven F, Heizmann CW, Brion JP. Astrocytic calcium/zinc binding protein S100A6 over expression in Alzheimer's disease and in PS1/APP transgenic mice models. Biochimica et Biophysica Acta (BBA) - Molecular Cell Research. 2004; 1742:161–168.
7. Brambilla R, Bracchi Ricard V, Hu WH, Frydel B, Bramwell A, Karmally S, Green E, Bethea J. Inhibition of astroglial nuclear factor kappaB reduces inflammation and improves functional recovery after spinal cord injury. The Journal of experimental medicine. 2005; 202:145–156. [PubMed: 15998793]
8. Bush TG, Puvanachandra N, Horner CH, Polito A, Ostenfeld T, Svendsen CN, Mucke L, Johnson MH, Sofroniew MV. Leukocyte infiltration, neuronal degeneration, and neurite outgrowth after ablation of scar-forming, reactive astrocytes in adult transgenic mice. Neuron. 1999; 23:297–308. [PubMed: 10399936]
9. Bushong EA, Martone ME, Jones YZ, Ellisman MH. Protoplasmic Astrocytes in CA1 Stratum Radiatum Occupy Separate Anatomical Domains. J Neurosci. 2002; 22:183–192. [PubMed: 11756501]
10. Bushong EM, Maryann|Ellisman Mark. Maturation of astrocyte morphology and the establishment of astrocyte domains during postnatal hippocampal development. International Journal of Developmental Neuroscience. 2004; 22:73–86. [PubMed: 15036382]
11. Chen MJ, Wong CH, Peng ZF, Manikandan J, Melendez AJ, Tan TM, Crack PJ, Cheung NS. A global transcriptomic view of the multifaceted role of glutathione peroxidase-1 in cerebral ischemic-reperfusion injury. Free Radic Biol Med. 2011; 50:736–748. [PubMed: 21193029]
12. Chiamulera C, Terron A, Reggiani A, Cristofori P. Qualitative and quantitative analysis of the progressive cerebral damage after middle cerebral artery occlusion in mice. Brain Research. 1993; 606:251–258. [PubMed: 7683958]
13. Correa-Cerro LSMDP, Mandell JWMDP. Molecular Mechanisms of Astrogliosis: New Approaches With Mouse Genetics. [Review]. Journal of Neuropathology & Experimental Neurology. 2007 Mar; 66(3):169–176. [PubMed: 17356378]
14. Currie RW, Karmazyn M, Kloc M, Mailer K. Heat-shock response is associated with enhanced postischemic ventricular recovery. Circulation Research. 1988; 63:543–549. [PubMed: 3409486]
15. De Paola M, Buanne P, Biordi L, Bertini R, Ghezzi P, Mennini T. Chemokine MIP-2/CXCL2, acting on CXCR2, induces motor neuron death in primary cultures. Neuroimmunomodulation. 2007; 14:310–316. [PubMed: 18391506]
16. Dennis G Jr, Sherman BT, Hosack DA, Yang J, Gao W, Lane HC, Lempicki RA. DAVID: Database for Annotation, Visualization, and Integrated Discovery. Genome Biol. 2003; 4:P3. [PubMed: 12734009]
17. Dienel GA, Hertz L. Astrocytic contributions to bioenergetics of cerebral ischemia. Glia. 2005; 50:362–388. [PubMed: 15846808]
18. Dingman A, Lee SY, Derugin N, Wendland MF, Vexler ZS. Aminoguanidine inhibits caspase-3 and calpain activation without affecting microglial activation following neonatal transient cerebral ischemia. Journal of Neurochemistry. 2006; 96:1467–1479. [PubMed: 16464234]
19. Eddleston M, Mucke L. Molecular profile of reactive astrocytes--Implications for their role in neurologic disease. Neuroscience. 1993; 54:15–36. [PubMed: 8515840]
20. Feng L, Hatten ME, Heintz N. Brain lipid-binding protein (BLBP): A novel signaling system in the developing mammalian CNS. Neuron. 1994; 12:895–908. [PubMed: 8161459]
21. Fernaud-Espinosa I, Nieto-Sampedro M, Bovolenta P. Differential activation of microglia and astrocytes in aniso- and isomorphic gliotic tissue. GLIA. 1993; 8:277–291. [PubMed: 8406684]

22. Fitch M, Silver J. CNS injury, glial scars, and inflammation: Inhibitory extracellular matrices and regeneration failure. Experimental neurology. 2008; 209:294–301. [PubMed: 17617407]
23. Gautier L, Cope L, Bolstad BM, Irizarry RA. affy--analysis of Affymetrix GeneChip data at the probe level. Bioinformatics. 2004; 20:307–315. [PubMed: 14960456]
24. Gentleman RC, Carey VJ, Bates DM, Bolstad B, Dettling M, Dudoit S, Ellis B, Gautier L, Ge Y, Gentry J, Hornik K, Hothorn T, Huber W, Iacus S, Irizarry R, Leisch F, Li C, Maechler M, Rossini AJ, Sawitzki G, Smith C, Smyth G, Tierney L, Yang JY, Zhang J. Bioconductor: open software development for computational biology and bioinformatics. Genome Biol. 2004; 5:R80. [PubMed: 15461798]
25. Giffard RG, Han RQ, Emery JF, Duan M, Pittet JF. Regulation of apoptotic and inflammatory cell signaling in cerebral ischemia: the complex roles of heat shock protein 70. Anesthesiology. 2008; 109:339–348. [PubMed: 18648242]
26. Giffard RG, Xu L, Zhao H, Carrico W, Ouyang Y, Qiao Y, Sapolsky R, Steinberg G, Hu B, Yenari MA. Chaperones, protein aggregation, and brain protection from hypoxic/ischemic injury 10.1242/jeb.01034. J Exp Biol. 2004; 207:3213–3220. [PubMed: 15299042]
27. Hamby M, Sofroniew M. Reactive astrocytes as therapeutic targets for CNS disorders. Neurotherapeutics. 2010; 7:494–506. [PubMed: 20880511]
28. Han RQ, Ouyang YB, Xu L, Agrawal R, Patterson AJ, Giffard RG. Postischemic brain injury is attenuated in mice lacking the beta2-adrenergic receptor. Anesth Analg. 2009; 108:280–287. [PubMed: 19095863]
29. Hausmann R, Betz P. Course of glial immunoreactivity for vimentin, tenascin and alpha1-antichymotrypsin after traumatic injury to human brain. International Journal of Legal Medicine. 2001; 114:338–342. [PubMed: 11508799]
30. Hayakawa K, Nakano T, Irie K, Higuchi S, Fujioka M, Orito K, Iwasaki K, Jin G, Lo E, Mishima K, Fujiwara M. Inhibition of reactive astrocytes with fluorocitrate retards neurovascular remodeling and recovery after focal cerebral ischemia in mice. Journal of cerebral blood flow and metabolism. 2010; 30:871–882. [PubMed: 19997116]
31. Hirose K, Chan PH. Blockade of glutamate excitotoxicity and its clinical applications. Neurochemical research. 1993; 18:479–483. [PubMed: 7682661]
32. Hoehn B, Ringer TM, Xu L, Giffard RG, Sapolsky RM, Steinberg GK, Yenari MA. Overexpression of HSP72 After Induction of Experimental Stroke Protects Neurons From Ischemic Damage. 2001; 21:1303–1309.
33. Hoyaux D, Boom A, Van den Bosch L, Belot N, Martin JJ, Heizmann CW, Kiss R, Pochet R. S100A6 Overexpression within Astrocytes Associated with Impaired Axons from Both ALS Mouse Model and Human Patients. Journal of Neuropathology & Experimental Neurology. 2002; 61:736–744. [PubMed: 12152788]
34. Huang da W, Sherman BT, Lempicki RA. Systematic and integrative analysis of large gene lists using DAVID bioinformatics resources. Nat Protoc. 2009; 4:44–57. [PubMed: 19131956]
35. Iwazaki T, McGregor IS, Matsumoto I. Protein expression profile in the striatum of rats with methamphetamine-induced behavioral sensitization. PROTEOMICS. 2007; 7:1131–1139. [PubMed: 17351886]
36. Lau LT, Yu AC. Astrocytes produce and release interleukin-1, interleukin-6, tumor necrosis factor alpha and interferon-gamma following traumatic and metabolic injury. J Neurotrauma. 2001; 18:351–359. [PubMed: 11284554]
37. Lee JM, Zipfel GJ, Choi DW. The changing landscape of ischaemic brain injury mechanisms. Nature. 1999; 399:A7–14. [PubMed: 10392575]
38. Lee WC, Wen HC, Chang CP, Chen MY, Lin MT. Heat shock protein 72 overexpression protects against hyperthermia, circulatory shock, and cerebral ischemia during heatstroke. J Appl Physiol. 2006; 100:2073–2082. [PubMed: 16627676]
39. Loddick SA, Turnbull AV, Rothwell NJ. Cerebral Interleukin-6 Is Neuroprotective During Permanent Focal Cerebral Ischemia in the Rat. J Cereb Blood Flow Metab. 1998; 18:176–179. [PubMed: 9469160]
40. Maragakis NJ, Rothstein JD. Mechanisms of Disease: astrocytes in neurodegenerative disease. 2006; 2:679–689.

41. Marber MS, Mestril R, Chi SH, Sayen MR, Yellon DM, Dillmann WH. Overexpression of the rat inducible 70-kD heat stress protein in a transgenic mouse increases the resistance of the heart to ischemic injury. J Clin Invest. 1995; 95:1446–1456. [PubMed: 7706448]
42. Niizuma K, Endo H, Chan PH. Oxidative stress and mitochondrial dysfunction as determinants of ischemic neuronal death and survival. J Neurochem. 2009; 109(Suppl 1):133–138. [PubMed: 19393019]
43. Parcellier A, Gurbuxani S, Schmitt E, Solary E, Garrido C. Heat shock proteins, cellular chaperones that modulate mitochondrial cell death pathways. Biochem Biophys Res Commun. 2003; 304:505–512. [PubMed: 12729585]
44. Pekny M, Nilsson M. Astrocyte activation and reactive gliosis. GLIA. 2005; 50:427–434. [PubMed: 15846805]
45. Perea G, Araque A. Astrocytes potentiate transmitter release at single hippocampal synapses. Science. 2007; 317:1083–1086. [PubMed: 17717185]
46. Perea G, Navarrete M, Araque A. Tripartite synapses: astrocytes process and control synaptic information. Trends in Neurosciences. 2009; 32:421–431. [PubMed: 19615761]
47. Plumier JC, Krueger AM, Currie RW, Kontoyiannis D, Kollias G, Pagoulatos GN. Transgenic mice expressing the human inducible Hsp70 have hippocampal neurons resistant to ischemic injury. Cell Stress Chaperones. 1997; 2:162–167. [PubMed: 9314603]
48. Rajdev S, Hara K, Kokubo Y, Mestril R, Dillmann W, Weinstein PR, Sharp FR. Mice overexpressing rat heat shock protein 70 are protected against cerebral infarction. Annals of Neurology. 2000; 47:782–791. [PubMed: 10852544]
49. Ridet JL, Privat A, Malhotra SK, Gage FH. Reactive astrocytes: cellular and molecular cues to biological function. Trends in Neurosciences. 1997; 20:570–577. [PubMed: 9416670]
50. Sarabi AS, Shen H, Wang Y, Hoffer BJ, Bäckman CM. Gene expression patterns in mouse cortical penumbra after focal ischemic brain injury and reperfusion. Journal of Neuroscience Research. 2008; 86:2912–2924. [PubMed: 18506852]
51. Schaffner AE, Ghesquiere A. The effect of type 1 astrocytes on neuronal complexity: a fractal analysis. Methods. 2001; 24:323–329. [PubMed: 11465997]
52. Smith DH, Chen XH, Pierce JE, Wolf JA, Trojanowski JQ, Graham DI, McIntosh TK. Progressive atrophy and neuron death for one year following brain trauma in the rat. Journal of neurotrauma. 1997; 14:715–727. [PubMed: 9383090]
53. Sofroniew MV. Reactive Astrocytes in Neural Repair and Protection. Neuroscientist. 2005; 11:400–407. [PubMed: 16151042]
54. Sofroniew MV. Molecular dissection of reactive astrogliosis and glial scar formation. Trends in Neurosciences. 2009; 32:638–647. [PubMed: 19782411]
55. Soltys Z, Ziaja M, Pawlinski R, Setkowicz Z, Janeczko K. Morphology of reactive microglia in the injured cerebral cortex. Fractal analysis and complementary quantitative methods. J Neurosci Res. 2001; 63:90–97. [PubMed: 11169618]
56. Stenzel-Poore MP, Stevens SL, Simon RP. Genomics of Preconditioning. Stroke. 2004; 35:2683–2686. [PubMed: 15459430]
57. Stenzel-Poore MP, Stevens SL, Xiong Z, Lessov NS, Harrington CA, Mori M, Meller R, Rosenzweig HL, Tobar E, Shaw TE, Chu X, Simon RP. Effect of ischaemic preconditioning on genomic response to cerebral ischaemia: similarity to neuroprotective strategies in hibernation and hypoxia-tolerant states. The Lancet. 2003; 362:1028–1037.
58. Tang Y, Lu A, Aronow BJ, Wagner KR, Sharp FR. Genomic responses of the brain to ischemic stroke, intracerebral haemorrhage, kainate seizures, hypoglycemia, and hypoxia. Eur J Neurosci. 2002; 15:1937–1952. [PubMed: 12099900]
59. Thomas PD, Campbell MJ, Kejariwal A, Mi H, Karlak B, Daverman R, Diemer K, Muruganujan A, Narechania A. PANTHER: a library of protein families and subfamilies indexed by function. Genome Res. 2003; 13:2129–2141. [PubMed: 12952881]
60. Thomas PD, Kejariwal A, Guo N, Mi H, Campbell MJ, Muruganujan A, Lazareva-Ulitsky B. Applications for protein sequence-function evolution data: mRNA/protein expression analysis and coding SNP scoring tools. Nucleic Acids Res. 2006; 34:W645–650. [PubMed: 16912992]

61. Tusher VG, Tibshirani R, Chu G. Significance analysis of microarrays applied to the ionizing radiation response. Proc Natl Acad Sci U S A. 2001; 98:5116–5121. [PubMed: 11309499]
62. van der Weerd L, Lythgoe MF, Badin RA, Valentim LM, Akbar MT, de Belleroche JS, Latchman DS, Gadian DG. Neuroprotective effects of HSP70 overexpression after cerebral ischaemia--an MRI study. Exp Neurol. 2005; 195:257–266. [PubMed: 15936758]
63. von Schantz C, Saharinen J, Kopra O, Cooper J, Gentile M, Hovatta I, Peltonen L, Jalanko A. Brain gene expression profiles of Cln1 and Cln5 deficient mice unravels common molecular pathways underlying neuronal degeneration in NCL diseases. BMC Genomics. 2008; 9:146. [PubMed: 18371231]
64. Wang X, Xu L, Wang H, Zhan Y, Puré E, Feuerstein GZ. CD44 deficiency in mice protects brain from cerebral ischemia injury. Journal of Neurochemistry. 2002; 83:1172–1179. [PubMed: 12437588]
65. White R, Jakeman L. Don't fence me in: harnessing the beneficial roles of astrocytes for spinal cord repair. Restorative neurology and neuroscience. 2008; 26:197–214. [PubMed: 18820411]
66. White R, McTigue D, Jakeman L. Regional heterogeneity in astrocyte responses following contusive spinal cord injury in mice. Journal of comparative neurology. 2010; 518:1370–1390. [PubMed: 20151365]
67. Wong AHC, Lipska BK, Likhodi O, Boffa E, Weinberger DR, Kennedy JL, Van Tol HHM. Cortical gene expression in the neonatal ventral-hippocampal lesion rat model. Schizophrenia Research. 2005; 77:261–270. [PubMed: 15890497]
68. Xing C, Lee S, Kim WJ, Jin G, Yang YG, Ji X, Wang X, Lo EH. Role of oxidative stress and caspase 3 in CD47-mediated neuronal cell death. Journal of Neurochemistry. 2009; 108:430–436. [PubMed: 19012741]
69. Xiong X, Barreto GE, Xu L, Ouyang YB, Xie X, Giffard RG. Increased Brain Injury and Worsened Neurological Outcome in Interleukin-4 Knockout Mice After Transient Focal Cerebral Ischemia. Stroke. 2011; 42:2026–2032. [PubMed: 21597016]
70. Xu L, Emery JF, Ouyang YB, Voloboueva LA, Giffard RG. Astrocyte targeted overexpression of Hsp72 or SOD2 reduces neuronal vulnerability to forebrain ischemia. Glia. 2010; 58:1042–1049. [PubMed: 20235222]
71. Xu L, Lee JE, Giffard RG. Overexpression of bcl-2, bcl-xL or hsp70 in murine cortical astrocytes reduces injury of co-cultured neurons. Neuroscience Letters. 1999; 277:193–197. [PubMed: 10626846]
72. Xu L, Voloboueva LA, Ouyang Y, Emery JF, Giffard RG. Overexpression of mitochondrial Hsp70/Hsp75 in rat brain protects mitochondria, reduces oxidative stress, and protects from focal ischemia. J Cereb Blood Flow Metab. 2009; 29:365–374. [PubMed: 18985056]
73. Xu L, Xiong X, Ouyang Y, Barreto G, Giffard R. Heat shock protein 72 (Hsp72) improves long term recovery after focal cerebral ischemia in mice. Neuroscience Letters. 2011; 488:279–282. [PubMed: 21108992]
74. Yaglom J, O'Callaghan-Sunol C, Gabai V, Sherman MY. Inactivation of dual-specificity phosphatases is involved in the regulation of extracellular signal-regulated kinases by heat shock and hsp72. Mol Cell Biol. 2003; 23:3813–3824. [PubMed: 12748284]
75. Yenari MA, Fink SL, Sun GH, Chang LK, Patel MK, Kunis DM, Onley D, Ho DY, Sapolsky RM, Steinbrg GK. Gene therapy with HSP72 is neuroprotective in rat models of stroke and epilepsy. Annals of Neurology. 1998; 44:584–591. [PubMed: 9778256]
76. Zamanian JL, Xu L, Foo LC, Nouri N, Zhou L, Giffard RG, Barres BA. Genomic Analysis of Reactive Astrogliosis. The Journal of Neuroscience. 2012; 32:6391–6410. [PubMed: 22553043]
77. Zheng Z, Kim JY, Ma H, Lee JE, Yenari MA. Anti-inflammatory effects of the 70 kDa heat shock protein in experimental stroke. J Cereb Blood Flow Metab. 2008; 28:53–63. [PubMed: 17473852]
78. Zou J, Wang YX, Dou FF, Lü HZ, Ma ZW, Lu PH, Xu XM. Glutamine synthetase down-regulation reduces astrocyte protection against glutamate excitotoxicity to neurons. Neurochemistry International. 2010; 56:577–584. [PubMed: 20064572]

Highlights

1. After stroke Hsp72 overexpression results in more down regulated genes relative to WT
2. More inflammation associated genes increase in WT mice
3. The density of reactive astrocytes is reduced with Hsp72 overexpression
4. Different phenotypes of reactive astrocytes in the penumbra are observed with time

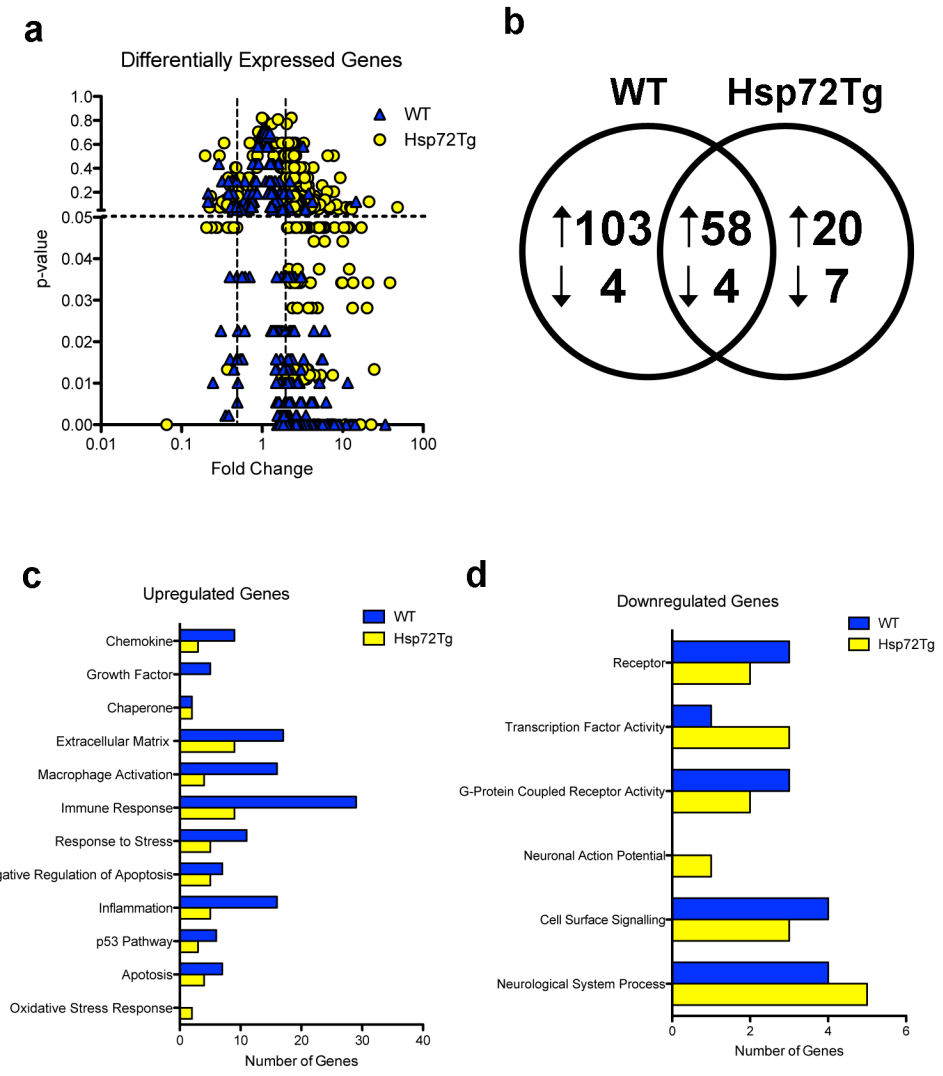

Figure 1.

Changes in gene expression 24h following MCAO in Hsp72Tg and WT mice. (a) Volcano plot showing genes up- or down-regulated at least 2-fold in either genotype, with p-value on the Y axis and fold change on the X axis. Dotted lines represents statistical cut-off at $p < 0.05$ and fold change at ≥ 2 and ≤ 0.5. (b) MCAO induces overlapping sets of genes in WT and Hsp72Tg mice. Venn diagram showing differentially regulated genes for each genotype, MCAO compared to sham. Arrows indicate the direction of change. (c–d) Over-represented gene ontology categories for the upregulated (c) and downregulated (d) genes. For each category and genotype, the number of genes is shown.

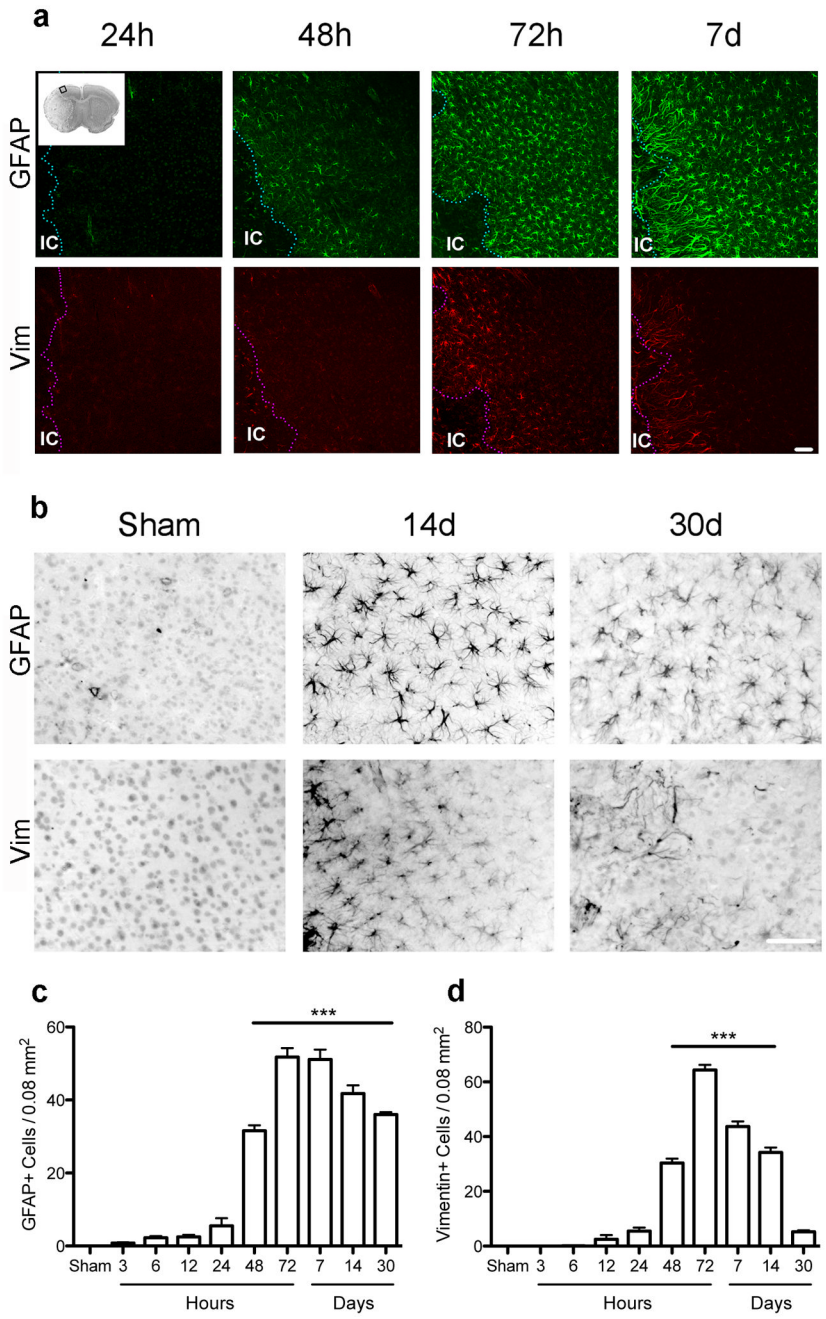

Figure 2.

Time course analysis of number of GFAP and Vim immunoreactive cells in the cortical penumbra through 1 month. (a) Low power view of GFAP and Vim expression in the cortical penumbra up to 1 week after stroke. Inset in top left image shows a cresyl violet stained section with a square indicating the cortical area where cell counting was performed. IC=ischemic core. (b) Representative micrographs show the relative number of cells per area at days 14 and 30. (c–d) Changes in the number of GFAP (c) and Vim (d) immunopositive cells varied through 30 days after injury. ***p<0.001 versus Sham. Scale bar = 50 μm. Graph shows mean +/− SEM.

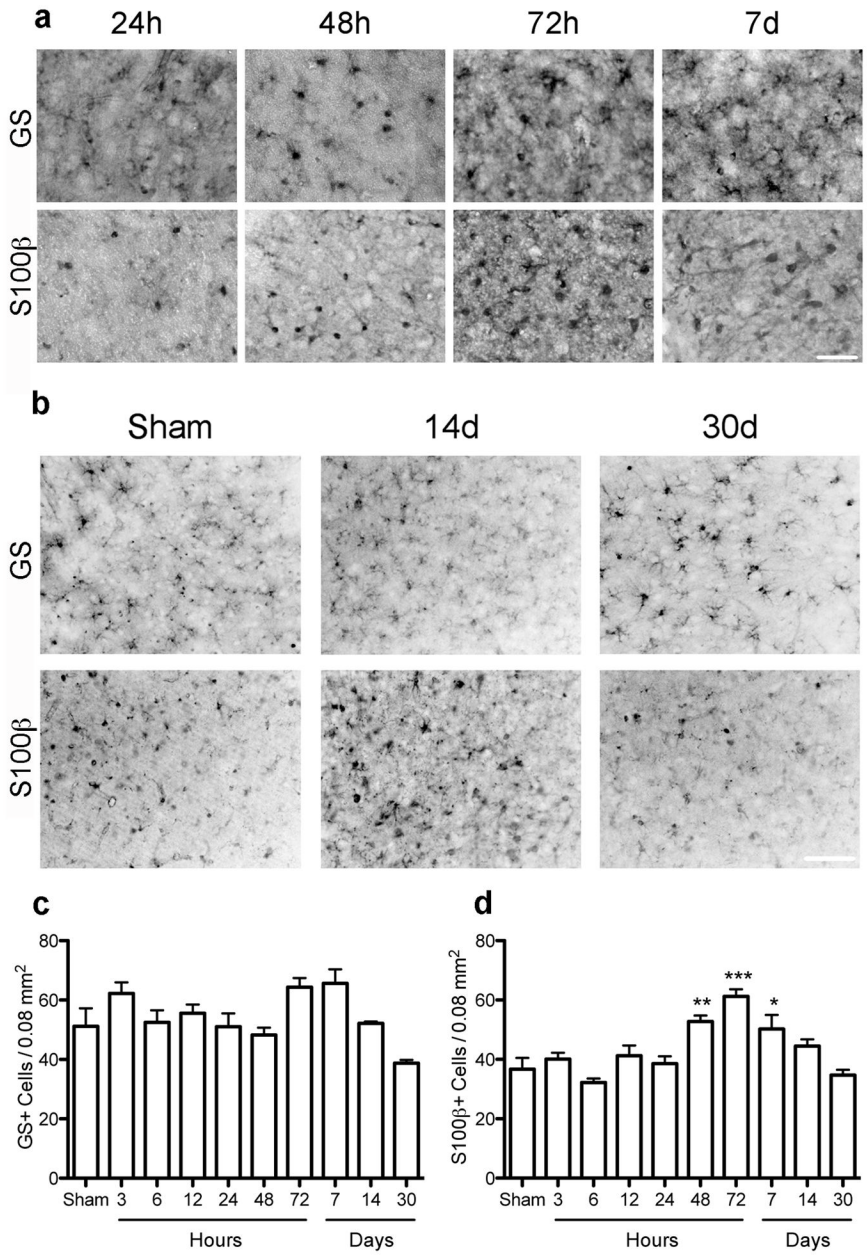

Figure 3.

The number of cells immunoreactive for GS or S100β show limited change in the cortical penumbra through 1 month. (a) Representative micrographs showing GS+ or S100β+ cell density in the cortical penumbra over time. (b) Representative micrographs show the relative number of cells per area at the late timepoints, days 14 and 30. (c, d) Quantitation of the density of GS- or S100β-immunoreactive astrocytes in the cortical penumbra showed no difference in number of GS+ cells over time compared to sham (c) and a moderate but significant increase in the number of $S100\beta^{+}$ astrocytes only at 2 – 7d following stroke (d). *p<0.05, **p<0.01, ***p<0.001 versus Sham. Scale bar = 50 μm. Graph shows mean +/− SEM.

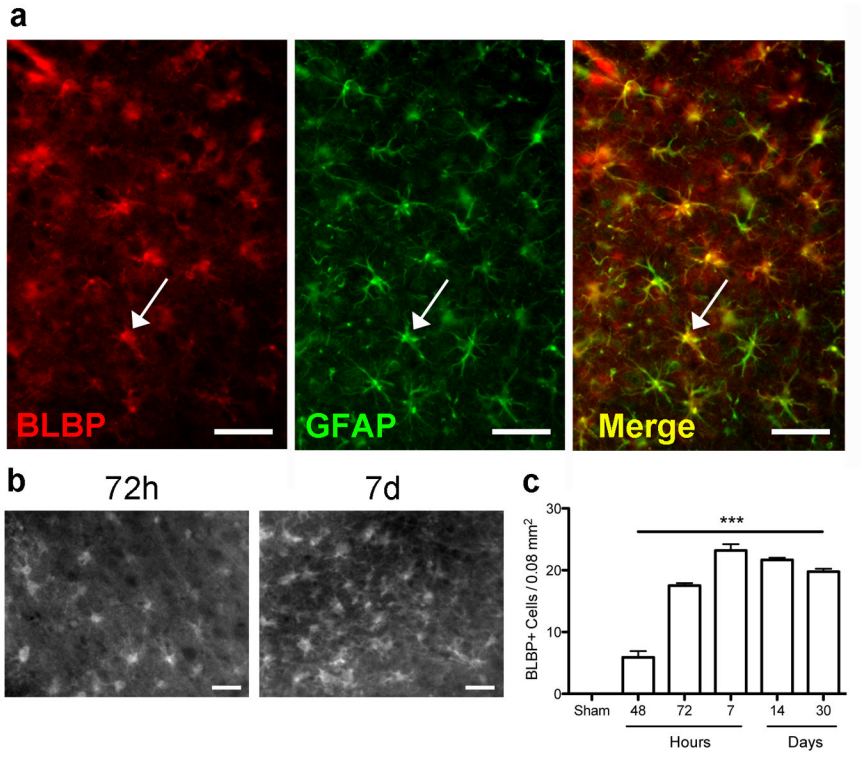

Figure 4.

The number of BLBP immunoreactive cells increases at 48h following MCAO and remains increased through 30 days. (a) Fluorescence micrographs show that BLBP colocalizes with GFAP at 72h following MCAO. Arrow indicates a single cell among the many showing colocalization, yellow on the merged image. (b) Micrographs of BLBP+ cells 72h and 7d after MCAO. (c) Quantification of BLBP-positive cells in the cortical penumbra, showing a significant increase at 48h that remains elevated through 30d. ***p<0.001 versus sham. Scale bar = 50 μm.

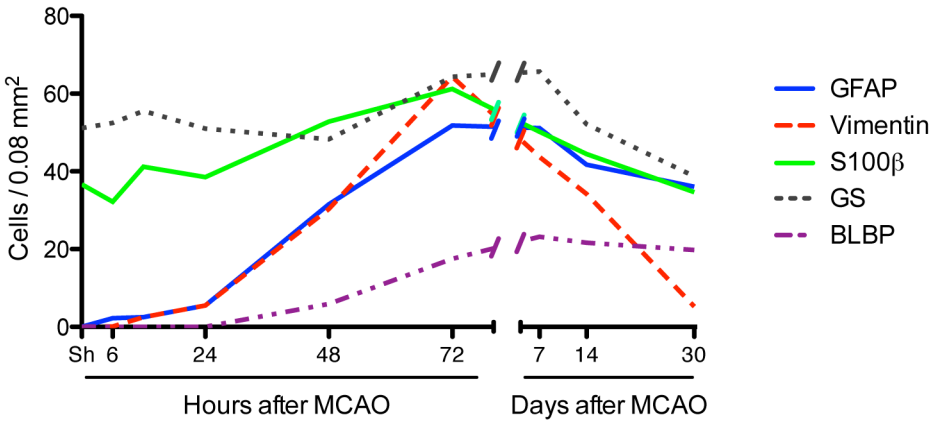

Figure 5.

Summary of time-dependent changes in astrocyte immunopositive density demonstrates 4 different patterns. While the number of cells expressing GFAP and BLBP peak on day 3 post MCAO and remain high, the number of Vim immunoreactive cells peaks at 72h and then declines sharply. S100β-positive cells increase only at intermediate times, 2–7 days, while GS numbers are not significantly different with time.

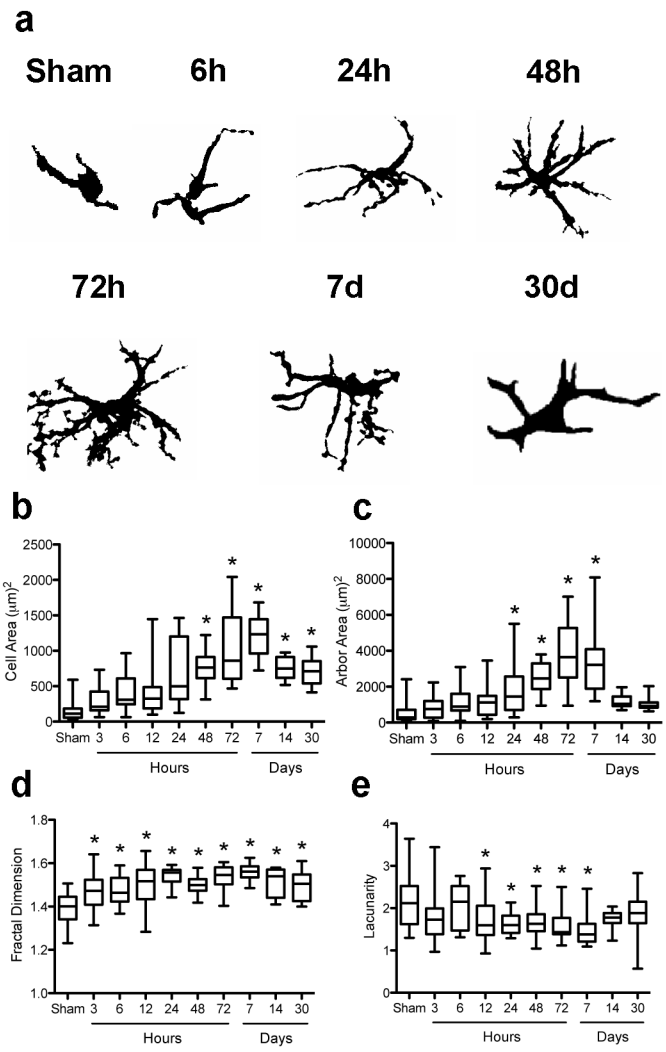

Figure 6.

Fractal analysis shows that astrocyte activation is characterized by changes in both the cell body and processes. (a) GFAP immunoreactive astrocytes display different morphological phenotypes with time after injury. Cell shape is progressively hypertrophied and more bushy with time. Significant alterations in astrocyte morphology are seen by fractal analysis at 48h, 72h and 7d, with increased cell (b) and arbor area (c), fractal dimension (d), and decreased lacunarity (e). *$p<0.05$ versus Sham. On the box plot, the line indicates the mean, the box represents the 25^{th} and 75^{th} percentile, and bars show minimum and maximum.

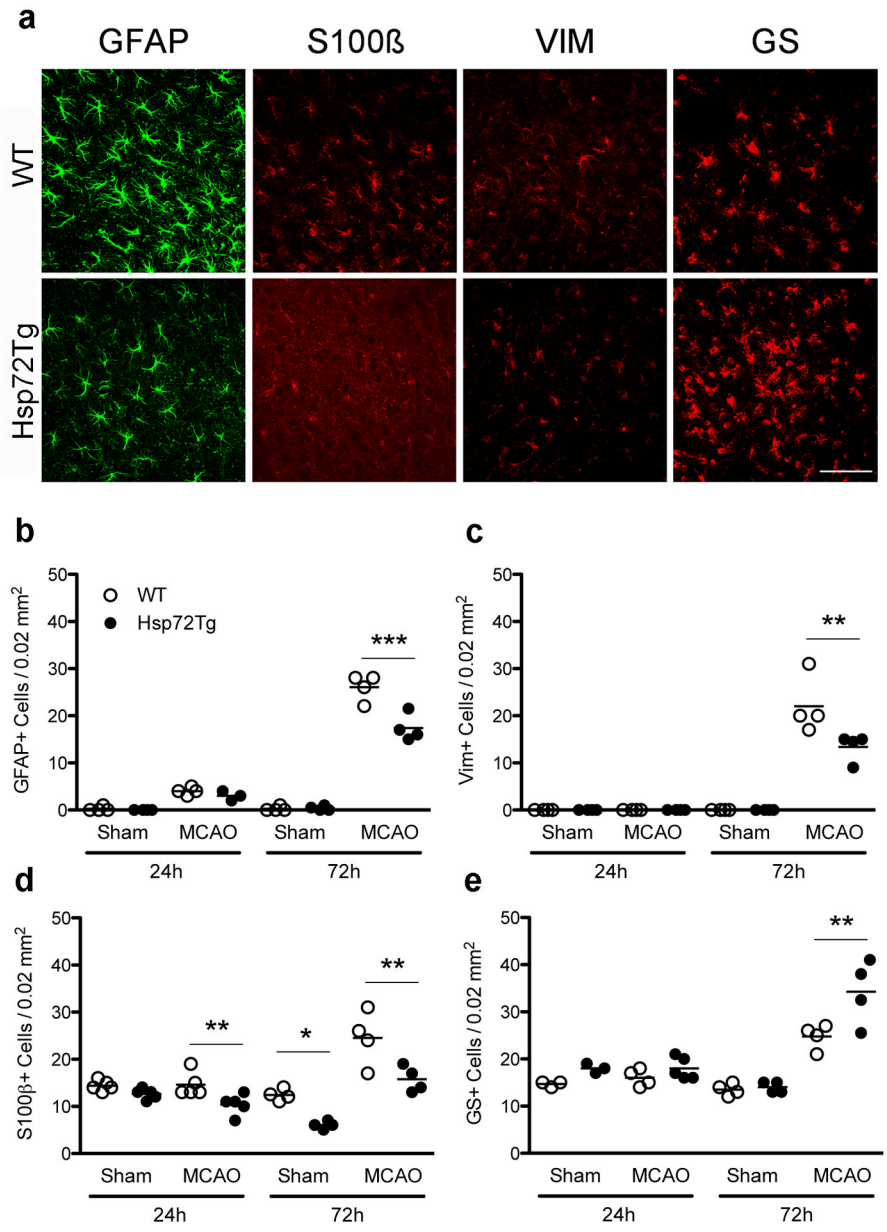

Figure 7.

Hsp72 overexpression affects changes in density of GFAP, Vim, S100β, or GS immunoreactive astrocytes assessed at 24 and 72h post MCAO. (a) Representative fluorescent micrographs of sections immunostained for these markers at 72 h after injury in WT and Hsp72Tg mice. The number of GFAP+ (b) and vimentin+ (c) astrocytes were lower in Hsp72Tg mice 72h following sham or MCAO surgery. (d) The number of S100β+ cells were significantly lower in Hsp72Tg mice compared to WT controls both at 24h and 72h following surgery (genotype difference of $p < 0.01$). (e) In contrast, Hsp72Tg mice exhibited significantly more GS+ cells 72h after surgery. Asterisks indicate significant differences between genotypes after *post hoc* analysis; *$p < 0.05$, **$p < 0.01$, ***$p < 0.001$. Scale bar = 50 μm. On graph, circles represent individual animals, and lines show the mean.

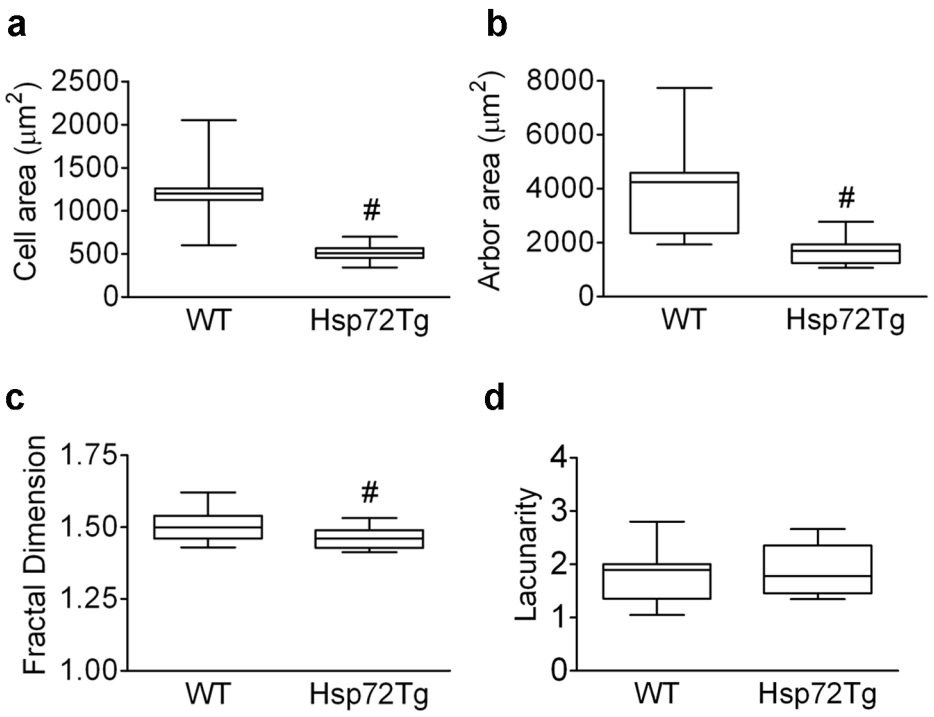

Figure 8.

Hsp72 overexpression alters astrocyte morphological changes quantitated by fractal analysis at 72h post MCAO. Significant differences were observed between genotypes in cell area (a), arbor area (b), and fractal dimension (c), but not lacunarity (d). #$p < 0.05$. On graph, line indicates mean, box represents the 25th and 75th percentile, and bars show minimum and maximum.

Table 1

Fold Change in Astrocyte-Associated Genes 24 hr after transient focal ischemia by genotype

Symbol	Description	WT	Hsp72Tg	References
Hmox1*	heme oxygenase (decycling) 1	5,98	8.45[a]	(Schipper et al., 2009)
Cxcl10*	chemokine (C-X-C motif) ligand 10	3,79	9.66	(Wang et al., 1998) (17510981)
Lcn2*	lipocalin 2	33.88	38.68	(Lee et al., 2009)
Cd14*	CD14 antigen	13.38	16.61	(Galea et al., 1996)
Socs3*	suppressor of cytokine signaling 3	12.78	22.63	(Okada et al., 2006)
Il6*	interleukin 6	12.38	20.14	(Lau and Yu, 2001; Van Wagoner et al., 1999)
Timp1*	tissue inhibitor of metalloproteinase 1	8.88	10.76	(Rivera et al., 1997)
Spp1*	secreted phosphoprotein 1	8.34	6.39 [a]	(Ellison et al., 1998)
Serpina3n*	serine (or cysteine) peptidase inhibitor, clade A, member 3N	7.59	6.89 [a]	(Rattner and Nathans, 2005)
Cxcl2*	chemokine (C-X-C motif) ligand 2	6.22	48.00 [a]	(Lu et al., 2005; Valles et al., 2006)
Serpine1*	serine (or cysteine) peptidase inhibitor, clade E, member 1	6.14	7.17	(Vivien and Buisson, 2000; Yepes and Lawrence, 2004a; Yepes and Lawrence, 2004b)
Ccl2*	chemokine (C-C motif) ligand 2	5.61	17.04	(Lawrence et al., 2006) (11384610)
Icam1*	intercellular adhesion molecule	4.81	11.59 [a]	(Yin et al., 2004) (785406)
Tgfbi	transforming growth factor, beta induced	4.55	7.52	(Meeuwsen et al., 2003)
Cd44*	CD44 antigen	4.39	5.27 [a]	(Girgrah et al., 1991; Haegel et al., 1993)
Vim*	Vimentin	4.38	4.79 [a]	(Calvo et al., 1991; Ridet et al., 1997)
S100a11	S100 calcium binding protein A11 (calgizzarin)	4.11	4.50 [a]	(Deloulme et al., 2000)
Igfbp3	insulin-like growth factor binding protein 3	3.98	4.44	(Keene et al., 2009; Mewar and McMorris, 1997)
Gfap*	glial fibrillary acidic protein	3.49	3.33 [a]	(Calvo et al., 1991; Ridet et al., 1997)
Osmr*	oncostatin M receptor	3.47	4.17	(Glezer and Rivest, 2010)
Thbd*	Thrombomodulin	3.41	3.72	(Pindon et al., 2000)
Akap12*	A kinase (PRKA) anchor protein (gravin) 12	3.21	5.03	(Lee et al., 2003)
Cxcl1*	chemokine (C-X-C motif) ligand 1	3.05	11.43	(Lu et al., 2005; Valles et al., 2006) (8152586)
Thbs1*	thrombospondin 1	2.52	3.08 [a]	(Lu and Kipnis, 2010) (12511771)
Cp*	Ceruloplasmin	2.45	2.35	(Hwang et al., 2004) (16542745)

This group of genes was assembled from literature showing that these genes were upregulated by astrocytes upon stress or in a neurodegenerative disease. Changes in their expression levels in each genotype after focal ischemia relative to sham treatment of the same genotype is shown. Fold change values with a superscript “a” indicate a nonsignificant ($p > 0.05$) increase from sham to MCAO. Genes with an asterisk (*) were also identified as upregulated specifically in astrocytes following MCAO by Zamanian et al. (2012).